Coupled Magnetic Field and Thermal Analysis Model for an IPMSM With Modular Three-Phase Winding Topologies for Fault-Tolerant Applications

SAYYED HALEEM SHAH[ID]1, XIAOYUAN WANG1, MUHAMMAD AZEEM[ID]2, AND USMAN ABUBAKAR1

1School of Electrical and Information Engineering, Tianjin University, Tianjin 300072, China
2Department of Electrical Engineering, Federal Urdu University of Arts, Science and Technology, Islamabad 45570, Pakistan

Corresponding author: Muhammad Azeem (engr.m.azeem786@gmail.com)

ABSTRACT Multi three-phase machines are frequently recommended for high current and high power applications due to their ability to minimize phase current while maintaining rated power and phase voltage. Furthermore, multi three-phase machines are also proposed because of their fault-tolerant capability to operate in partial working conditions due to their redundant structure. A partial working condition may occur when one or more three-phase winding sets go into faulty condition. This article focuses on evaluating the thermal behavior and efficiency of a multi three-phase machine comprising different modular winding topologies to investigate its normal, partial, and partially overloaded operation. The machine prototype used in the analysis is an interior permanent magnet synchronous machine (IPMSM) having six three-phase winding sets configured in modular three-phase winding arrangements. Firstly, the prototype machine's losses, efficiency, and output torque performances are evaluated through electromagnetic finite element analysis (FEA) for the different modular three-phase winding topologies applying similar operating conditions. Then the machine's thermal behavior is evaluated for the modular (concentrated, distributed, and combined concentrated and distributed) three-phase winding topologies through a coupled magnetic field and thermal analyses under the machine's healthy, partial, and partially overload operations. Finally, a comparative thermal analysis is presented for the machine prototype along with experimental validations for the analyzed modular three-phase windings topologies. This research study suggests the best modular three-phase winding topology for a multi three-phase machine considering efficiency performance and mutual heat exchange phenomenon between different three-phase independent winding sets, particularly for the machine's partial and partially over-load working conditions.

INDEX TERMS Interior permanent magnet synchronous machine, winding topologies, thermal analysis, fault-tolerance, lumped parameter thermal network, sensitivity analysis.

I. INTRODUCTION

Multi three-phase machines equipped with modular three-phase winding sets have attracted many research studies recently. They are considered an exciting and viable design choice, mainly due to their standout advantages of power splitting, low torque ripple, fault-tolerance, and their extensive usage in safety-critical and fault-tolerant

The associate editor coordinating the review of this manuscript and approving it for publication was Atif Iqbal[ID].

applications [1]–[5]. Similarly, the modular stator winding topology of the multi three-phase machines also allows the reduction of phase current without increasing the voltage per phase for a given rated power, particularly in high power systems like hybrid aircraft, wind generation, turbo compressors, and many other industrial applications [6]–[9]. The redundant structure of multi three-phase machines enables the partial operating capability of the machine under open-circuit fault-tolerant conditions. The partial operating state of the machine drive happens when one or more

three-phase winding sets are switched off due to phase faults, while the remaining three-phase winding sets continuously operate the machine drive.

Recently the focus of research has mainly been on the design, modelling, radial forces, and electromagnetic considerations of multi three-phase machines [10]. However, thermal analysis of electrical machines has obtained more attention during the last few decades since it directly influences the machine's power density, reliability, and overall efficiency. Moreover, the machine's thermal characteristics, along with its designed cooling technique, directly impact its loading capability. The winding insulation can be severely damaged, resulting in thermal ageing and critical machine failures due to the thermal overload operation of an electric machine. Henceforth, thermal analysis of an electric machine plays a critical role, particularly under short-time load, overload, or fault-tolerant operating conditions.

Meanwhile, the thermal behavior of multiphase machines has been investigated in many existing research studies [11]–[13]; however, there are very limited contributions to the research study on the thermal investigation of multi three-phase machines. [14] Discusses the electromagnetic design and performance evaluation of the dual three-phase machine, while [15] and [16] presents a detailed investigation about the radial forces and torque response of multi-sector machine design and its electromagnetic considerations. The multi-sector machine has a multi three-phase winding arrangement in which each three-phase winding set is located in separate sectors of the stator. Similarly, the thermal behavior of multi-sector machines has been discussed, and a detailed thermal study is presented in literature considering the sector design approach of multi three-phase machines [17]–[23].

The existing literature, to the best of the author's knowledge, offers limited research regarding different modular three-phase winding topologies and their impact on multi three-phase machine's efficiency performance and thermal behavior under healthy and particularly under partial and partial overload working conditions. Therefore the primary goal of this study is to evaluate the thermal behavior of the multi three-phase modular IPMSM by analyzing different modular three-phase winding topologies. Firstly, the machine's electromagnetic performance is evaluated using FEA for the analyzed modular winding topologies applying similar working conditions. The machine efficiency and losses are calculated then coupled to the thermal model for the investigation of its thermal response. The machine's thermal response is studied for three different types of multi three-phase winding topologies under healthy as well as the partial and partially overloaded working operation applying the coupled electromagnetic-thermal analyses technique. The overloaded thermal behavior of the machine is also investigated for the analyzed winding topologies, and an optimized machine model is designed based on thermal parametric sensitivity analysis. Lastly, a brief comparison and experimental test validations are presented.
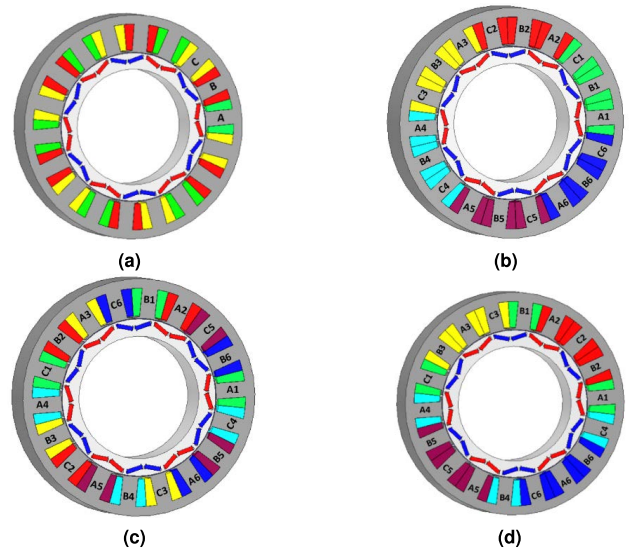

FIGURE 1. Machine model (a) Three-phase winding (b) Concentrated modular three-phase winding(c) Distributed modular three-phase winding (d) Combined concentrated and distributed modular three-phase winding.

II. MODULAR THREE-PHASE WINDING TOPOLOGIES AND MACHINE STRUCTURE

Figure 1 presents the machine prototype used in this analysis having 18 slots and 12 rotor poles with modular three-phase winding topologies. The stator windings for the standard three-phase IPMSM shown in Figure 1(a) are reconfigured to have modular three-phase winding topologies, with each three-phase winding set having an independent, neutral point.

Figure 1(b) presents the concentrated modular three-phase winding topology with each three-phase winding set placed in separate portions without any overlapping with the other three-phase winding sets. This type of modular three-phase winding topology has the advantage of reducing mutual coupling between each independent three-phase winding set. Figure 1(c) presents the distributed modular three-phase winding topology having independent three-phase sets spread around the circumference of the machine stator. The third type of investigated modular three-phase winding topology is the combined concentrated and distributed modular three-phase winding topology, as shown in Figure 1(d). It combines both concentrated and distributed modular three-phase independent winding sets uniformly distributed along the machine stator. The basic parameters for the machine design are presented in Table 1.

III. MACHINE'S ELECTROMAGNETIC PERFORMANCE AND LOSS ANALYSES UNDER DIFFERENT WINDING TOPOLOGIES

A. ELECTROMAGNETIC PERFORMANCE EVALUATION

It can be observed from the modular winding arrangements in Figure 1 that the prototype fractional slot interior permanent magnet synchronous machine has 18 phases, allowing six independent three-phase inverters to control each

Parameters	Values	Parameters	Values
Rated power	35 (kW)	Rated speed	3600 rpm
Outer radius (stator)	300 (mm)	Stator slots	18
Inner radius (stator)	200 (mm)	Rotor poles	12
Air gap	0.9 mm	DC voltage	332 (V)
Stator tooth (width)	19.7 (mm)	Rated current	77A (RMS)
Machine axial length	60 (mm)	PM's material	N35UH
Number of turns/phase	17	Stator and Rotor material	M350-35A

machine unit independently under both normal and partial working conditions. The independent three-phase units can be supplied in exactly the same manner as their three-phase counterpart shown in Figure 1(a). In this kind of modular machine design, the only difference is in the winding topology location for each three-phase winding set which contributes equally to the total air gap magnetic field under normal operating conditions. Finite element analysis (FEA) is used to investigate the electromagnetic performance analyses of the analyzed machine model. A comprehensive FEA is conducted to investigate the magnetic field distribution in the machine air gap for the concentrated modular three-phase winding topology, and the machine's distributed modular three-phase winding topology.

The corresponding waveform comparison plots of the machine radial flux density and their comparative harmonic spectrum plots for both the modular three-phase winding topologies under the machine's normal and partial working cases are shown in Figure 2. The radial flux density waveform for the machine's normal working case under modular three-phase winding sets, along with their harmonic spectrum plots, are shown in Figures 2(a) and 2(b). Similarly, the corresponding radial flux density and their harmonic spectrum plots for the machine's prototype partial working conditions under modular concentrated as well as modular distributed three-phase winding topologies are subsequently shown in Figure 2.

B. GENERATED TORQUE UNDER NORMAL AND PARTIAL OPERATION

The significant advantage of a modular winding design approach is its ability to output torque even when some three-phase winding sets have a fault, and the machine operates partially, which is not possible in other normal machine designs. Figures 3(a) and 3(c) show the average torque waveform under the prototype machine's normal and partially working cases for the concentrated and distributed modular three-phase winding sets. Similarly, the machine's average torque against the varying amplitude of the current waveform is shown in Figures 3(b) and 3(d) for both modular winding topologies under normal and partial operations.

The machine's iron core magnetic saturation makes the torque waveform slowly non-linear with increasing current. The generated torque under normal working conditions
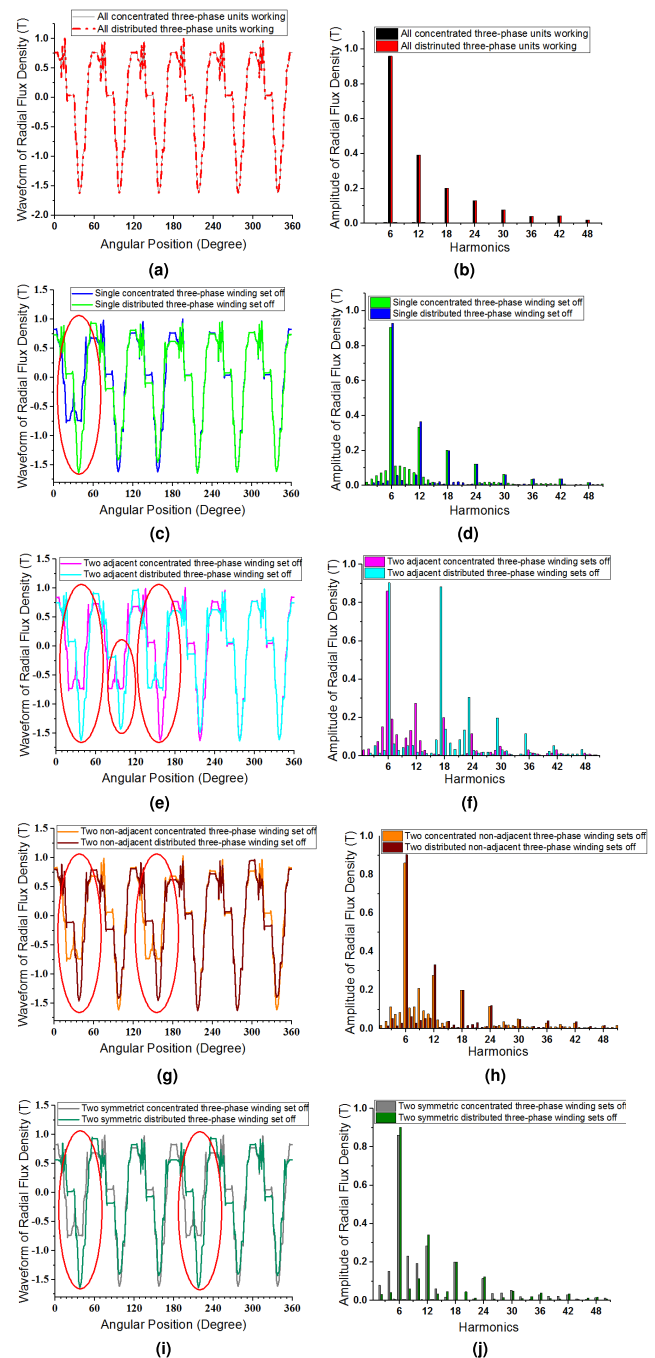

FIGURE 2. Flux density and harmonic spectrum plots for concentrated and distributed modular three-phase winding sets (a) Flux density under normal condition (b) Harmonic spectrum under normal condition (c) Flux density under a single winding set fault (d) Harmonic spectrum under a single winding set fault (e) Flux density under two adjacent winding sets fault (f) Harmonic spectrum under two adjacent winding sets fault (g) Flux density under two non-adjacent winding sets fault (h) Harmonic spectrum under two non-adjacent winding sets fault (i) Flux density under two symmetric winding sets fault (j) Harmonic spectrum under two symmetric winding sets fault.

is exactly the same for both winding topologies operated under the same conditions. However, the generated torque is always related to the number of healthy three-phase

TABLE 2. Average torque and torque ripple in concentrated and distributed three-phase winding topologies under normal and partial operation.

| Machine operating conditions at rated current 77A (RMS)	Average Torque concentrated three-phase sets	Average Torque distributed three-phase sets	% Torque Ripples concentrated three-phase sets (peak-to-peak)	% Torque Ripples distributed three-phase sets (peak-to-peak)	% Difference in Torque Ripples
All three-phase windings working	93.1	93.1	0.107	0.107	0
Single three-phase winding off	77.7	75.7	0.098	0.141	43.8
Two adjacent three-phase windings off	62.1	60.9	0.077	0.144	87
Two non adjacent three-phase windings off	62.2	60.5	0.095	0.114	51.5
Two symmetric three-phase windings off	62.3	60.7	0.094	0.169	79.7
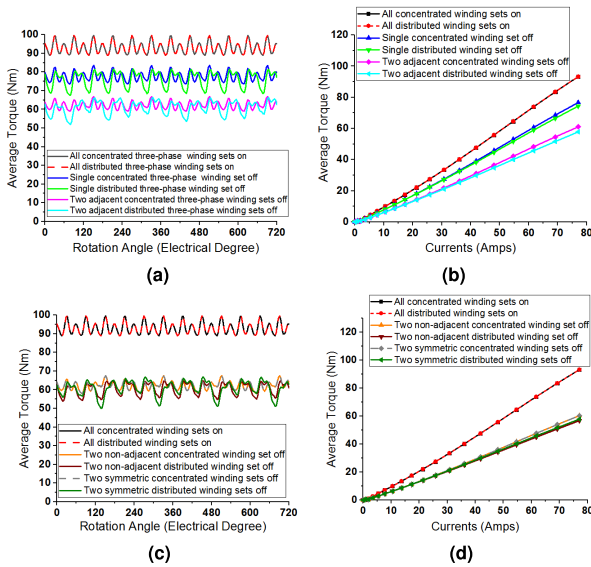
FIGURE 3. Comparison of average torque (a) Normal, single, and two adjacent three-phase sets off (b) Average torque against varying current under normal, single, and two adjacent three-phase sets off (c) Two non-adjacent and two symmetric three-phase sets off (d) Average torque against varying current under two non-adjacent and two symmetric three-phase sets off.

machine units operating under partial working conditions depending on the spatial position of the three-phase winding sets. Likewise, the generated average torque is different for the machine's concentrated and distributed modular three-phase winding topologies by applying similar operating conditions.

This analysis investigates four different partial working conditions for both winding topologies. The four analyzed partial working conditions have a single, two adjacent, two non-adjacent, and two symmetrical three-phase winding sets under open-circuit faults. The average torque and the torque ripples for both winding topologies under the normal and partially working cases are presented in Table 2. The torque data from Table 2 shows that under the same operating conditions (same supply current), the average output torque is comparatively less and the peak to peak torque ripples is higher for the distributed modular three-phase winding topology compared to the concentrated modular three-phase winding topology under the machine's partial working conditions.

Similarly, the efficiency maps for the machine prototype operating over a wide speed range are shown in Figure 4a and

4b for the investigated modular winding topologies operating under normal and partial conditions. It can be observed that the efficiency performance is comparatively higher for the machine design with concentrated modular three-phase winding topology compared to the same machine design with distributed modular three-phase winding topology under partial working conditions.

C. MACHINE's LOSS CALCULATIONS UNDER MODULAR THREE-PHASE WINDING TOPOLOGIES

In thermal analysis, the accurate calculation of losses is of great importance, same as finding the heat sources. This section presents the analytical methods and finite element analysis of the prototype machine losses under different winding topologies. Copper, iron, and permanent magnet losses are considered the main causes of temperature rise inside an electric machine. The copper losses P_c due to the armature windings for the machine winding sets can be calculated as

$$\begin{cases} P_C = mI_{rms}^2 R_{ph} \\ R_{ph} = R_{ph_0}(1 + S_R(T - T_{am})) \end{cases} \quad (1)$$

Here I_{rms} represent the (RMS) phase current, and R_{ph} represents the phase resistance, while m represents phase number. The resistance R_{ph_0} represents the phase resistance at $25°C$ ambient temperature T_{am}, with S_R representing the temperature coefficient. Eddy current losses and ohmic losses comprise the bulk of copper losses, with eddy current losses influenced by the skin effect, internal closeness, and contributions from magnetic time-varying fields. In contrast, ohmic losses are influenced by their resistive nature and temperature fluctuations, as described by (2). The permanent magnets (PM's) losses can be calculated using the expression given by

$$P_{PM} = \alpha/24 L_{PM} W_{PM} T_{PM} B f^2 \quad (2)$$

The length, width, and thickness of the PM are represented by L_{PM}, W_{PM}, and T_{PM}, respectively, while the magnetic flux density is represented by α and the applied current frequency is represented by f, respectively. Since the PM's sensitivity to temperature changes is high, therefore at high temperatures, irreversible demagnetization may occur. The B-H curve can be used to calculate the magnetic flux density; while having the values for the magnetic remanence and coercive force at an initial reference temperature. The variation of the magnetic flux density

TABLE 3. Properties of the material used in thermal analysis.

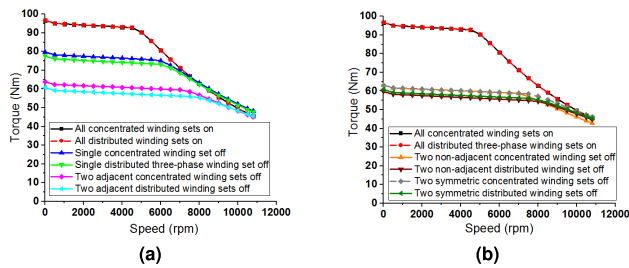| Machine parts	Density (kg/m^3)	Specific heat $(j/kg/°C)$	Thermal Conductivity
Stator	7650	460	30
Rotor	7650	460	30
Winding coils	8933	385	401
Shaft	7800	440	80
PM's	7500	460	7.6
Ambient Air	1.26	1000	0.125

FIGURE 4. Efficiency maps for concentrated and distributed modular winding topologies (a) Normal, single, and two adjacent three-phase sets off (b) Two non-adjacent and two symmetric three-phase sets off.

with temperature can be obtained using the expression below

$$B_r(T) = B_r(T_{ini_{ref}})[1 + \gamma(T - T_{ini_{ref}})] \quad (3)$$

$$H_c(T) = H_c(T_{ini_{ref}})[1 + \beta(T - T_{ini_{ref}})] \quad (4)$$

Here the magnetic remanence is represented by $B_r(T)$, with $H_c(T)$ representing the coercive force, while $T_{ini_{ref}}$ represents the initial reference temperature with γ and α representing the temperature coefficients. The core loss P_{core} can be represented by applying the Bertotti core loss model as in [14].

$$P_{core} = K_{hys}fB_{max}^n + K_{eddy}f^2B_{max}^2 + K_{ex}f^{1.5}B_{max}^{1.5} \quad (5)$$

Here, K_{hys}, represents the coefficient of hysteresis loss K_{eddy}, the eddy loss, and and K_{ex} represents excess loss coefficient. The amplitude of the magnetic flux density is represented by B, while f represents the fundamental AC magnetization frequency in [Hz]. The loss coefficients (K_{hys}, K_{eddy} and K_{ex}) can be calculated using the least-squares method based on the core loss characteristic of silicon steel, as shown in Table 3. The core losses are calculated at different rotation speeds using 2D-FEM in time-domain calculations, taking into account the magnetic flux density harmonics. The efficiency performance plots for the concentrated and distributed modular three-phase winding topologies are presented in Figure 4 applying the machine loss model. Similarly, the corresponding plots of the loss proportion for the machine under concentrated and distributed modular three-phase winding topologies are illustrated in Figure 5 and Figure 6, respectively.
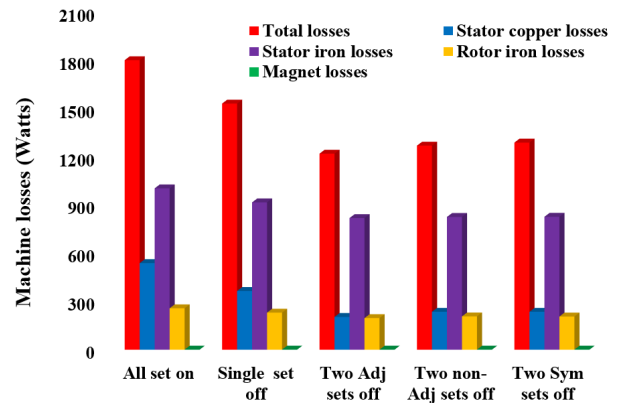

FIGURE 5. Machine's loss with concentrated modular three-phase winding units under normal and partial operating conditions.
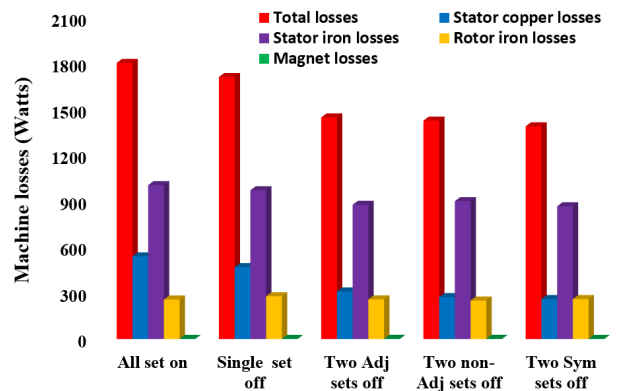

FIGURE 6. Machine's loss with distributed modular three-phase winding units under normal and partial operating conditions.
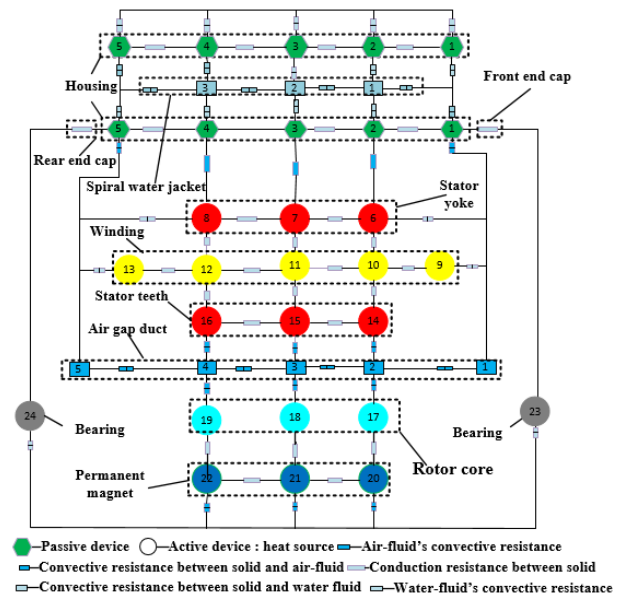

FIGURE 7. Lumped parameter thermal network for the machine.

IV. MACHINE's LUMPED PARAMETER THERMAL NETWORK (LPTN) MODEL

Heat is generated within the machine model as a result of losses; however, by constructing an effective cooling system,

the heat produced can be easily dispersed outside. A well-built cooling system alleviates the problem of temperature rise by providing adequate heat dissipation. By applying the loss calculation model mentioned above, a water-jacket cooling system is designed following the prototype machine model's key thermal nodes, using the lumped parameter thermal network (LPTN) model, as shown in Figure 7. The thermal analysis technique using an LPTN for an electric machine has proven reliable due to its quick processing time. Applying the LPTN model, the heat transfer equation in each node are presented below

$$P_i = \sum_{j \neq 1} (T_i - T_j) G_{i,j} = C_i \frac{dT_i}{dt} \qquad (6)$$

The generated heat is given by P_i, while the thermal capacitance is given by C_i at the i_{th} node, whereas the temperatures at the i_{th} and j_{th} nodes are T_i and T_j. $G_{(i,g)}$ presents the i_{th} and j_{th} nodes mutual thermal conductance. Under steady-state temperature conditions, the heat transport equation (6) can be reduced into a matrix form representation, as shown below

$$\begin{bmatrix} \sum_{j\neq1} G_{1,j} \ldots - G_{1,N} \\ \vdots \ddots \vdots \\ -G_{N,1} \ldots \sum_{j\neq N} G_{N,j} \end{bmatrix} * \begin{bmatrix} T_1 \\ \vdots \\ T_n \end{bmatrix} = \begin{bmatrix} P_1 \\ \vdots \\ P_n \end{bmatrix} \qquad (7)$$

Here $G_{i,j}$ represents a symmetric sparse matrix $\mathbf{G}$. As a result, the transient temperature rise and the steady-state nodal temperature distribution can be expressed as

$$\mathbf{T} = \mathbf{G}^{-1}\mathbf{P} \qquad (8)$$

$$\frac{ds}{dt} = (\mathbf{MC})^{-1}\mathbf{P} - (\mathbf{MC})^{-1}\mathbf{GT} \qquad (9)$$

Here $\mathbf{M}$ represents the matrix for the material mass in $[kg]$, $\mathbf{C}$ represents the specific heat $[J/(kgK)]$ matrix, and $\mathbf{T}$ represents column vector for temperature distribution at each node in $[°C]$. Generally, matrix $\mathbf{T}$ changes with time t, specified in (9) as a short step that discretizes the continuous equation allowing $T_{i,j}(k+1)$ to be replaced by $T_{i,j}(k)$. Henceforth, an analytical equation for the matrix differential solution can be expressed by

$$T(\mathbf{t}) = eA^{(t-t_0)} T_{i,j}(t_0) + \mathbf{A}^{-1}(e^{\mathbf{A}(t-t_0)} - I)\mathbf{B} \qquad (10)$$

Here $\mathbf{I}$ represents the unit matrix, while matrix $\mathbf{A}$ and vector $\mathbf{B}$ can be calculated as

$$\begin{cases} \mathbf{A} = -(\mathbf{MC})^{-1}\mathbf{G} \\ \mathbf{B} = (\mathbf{MC})^{-1}\mathbf{P} \end{cases} \qquad (11)$$

The column vector $\mathbf{P}$ also changes with respect to time t in the coupled magnetic field and thermal model transient analysis. If we assume that $\mathbf{P}$ is expressed using a linear interpolation approach [14], we get

$$\mathbf{P}(t) = \mathbf{K} \cdot t + \mathbf{P}_0 \qquad (12)$$

TABLE 4. Thermal parameters characteristics.

Parameters	Value
Windings thermal conductivity ($W/m/°C$)	0.3
Housing surface natural convection heat coefficient ($W/m^2/°C$)	0.08
Heat transfer coefficient for air inside ($W/m^2/°C$)	1.3

Here $\mathbf{K}$ represents the slope vector, while $\mathbf{P}_o$ is the column vector for the initial loss values. Similarly, also vector $\mathbf{B}$ changes with time; hence (10) can be expressed by

$$T(\mathbf{t}) = eA^{(t-t_0)} T(t_0) + \mathbf{A}^{-1}(e^{\mathbf{A}(t-t_0)} \mathbf{B}t_0 - \mathbf{B}(t))$$
$$+ \mathbf{A}^{-2}(e^{\mathbf{A}(t-t_0)} - I)\mathbf{D} \qquad (13)$$

Here $\mathbf{D}$ matrix and vector $\mathbf{B}(t)$ can be calculated as

$$\begin{cases} \mathbf{B}(t) = -(\mathbf{MC})^{-1}\mathbf{P}(t) \\ \mathbf{D} = (\mathbf{MC})^{-1}\mathbf{K} \end{cases} \qquad (14)$$

The distribution of the steady-state temperature can be obtained using equation (9), while transient temperature distribution can be obtained using (11) to (14). The above solutions can be implemented using commercial software, such as Matlab.

A. THERMAL RESISTANCE (CONDUCTION)

The conduction and convection thermal resistances are the most significant coefficients for the conductance matrix G presented in (8). All entities of the machine prototype have conductive heat transmissions, such as the stator, armature coil, rotor, PMs, iron laminations, etc. Therefore the internode (conduction) thermal resistance in the same state is given by

$$R(x, y) = \frac{D_{xy}}{\alpha A} \qquad (15)$$

Here D_{xy} represents the internode conduction distance between node x and y, while α represents the material thermal conductivity. The conduction path cross-sectional area is given by A in $[m^2]$.

B. THERMAL RESISTANCE (CONVECTION)

Natural and forced convection are the two main types of heat transfer between any solid and a fluid medium. As a result, the convection thermal resistance between two nodes under different conditions can be written as follows

$$R(u, v) = \frac{1}{h_\sigma A} \qquad (16)$$

Here, h_σ represents the heat transfer coefficient among the solid and the fluid contact region. Table 4 presents the thermal resistances for the key machine parts.

V. MACHINE's COUPLED MAGNETIC FIELD AND THERMAL MODEL UNDER DIFFERENT WINDING TOPOLOGIES

A coupled magnetic field and thermal network model is developed using the magnetic field loss calculation model
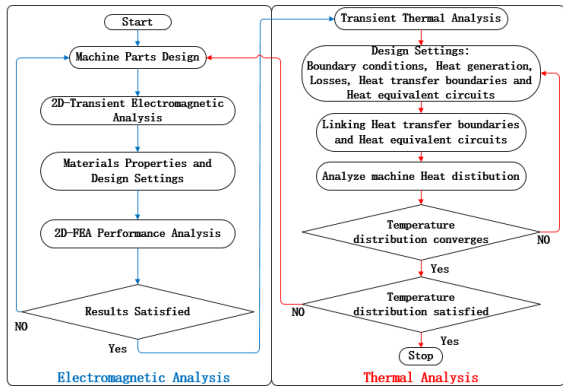
FIGURE 8. Coupled magnetic field and thermal analysis flow chart.

FIGURE 9. Windings hotspot temperature under same current supply for normal, single, and two adjacent three-phase winding sets partial operation.

FIGURE 10. Windings hotspot temperature under same current supply for two non-adjacent and two symmetric three-phase winding sets partial operation.

FIGURE 11. Windings hotspot temperature under same efficiency level for normal, single, and two adjacent three-phase winding sets partial operation.

from section III and the LPTN model presented from section IV to explore the thermal characteristics of the machine under modular three-phase winding topologies. An iteration technique is used to achieve bi-directional coupling to feedback the real-time output in the coupled magnetic field and LPTN model, as shown by the flow chart in Figure 8. Furthermore, the thermal behavior of the prototype machine with modular three-phase winding topologies is investigated based on the coupled magnetic field and LPTN model under normal and partial operating conditions as presented below.

A. MACHINE's THERMAL BEHAVIOR UNDER NORMAL AND PARTIAL OPERATION WITH MODULAR THREE-PHASE WINDING TOPOLOGIES

The machine prototype thermal behavior is examined for the concentrated modular three-phase windings topology under normal healthy operation, followed by the distributed modular three-phase winding topology using the coupled magnetic field and thermal network model. It can be observed from Figure 9 that the machine prototype thermal behavior under the same working condition for both modular three-phase winding topologies is found to be the same under normal healthy operation (all three-phase winding sets operational and supplied with the same current). However, the machine prototype thermal behavior under partial operation (some three-phase winding sets off) for the analyzed modular three-phase winding topologies is considerably different, as also mentioned in their efficiency analysis comparison presented in section III.

The phase currents in the distributed modular three-phase winding topology need to be increased to get the same efficiency level as the concentrated modular three-phase winding topology. Figure 9 presents the machine prototype temperature distributions for the winding hotspots under normal and partial operation (single, two adjacent three-phase winding sets off). The temperature results are obtained by supplying the modular three-phase winding sets with the same currents for both the concentrated and distributed modular three-phase winding topologies.
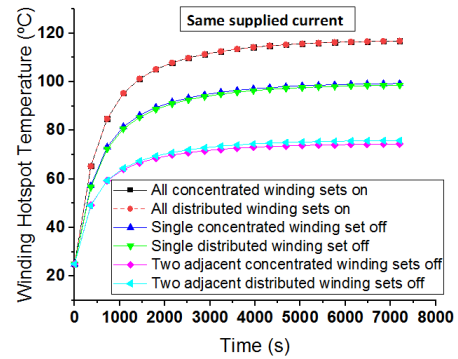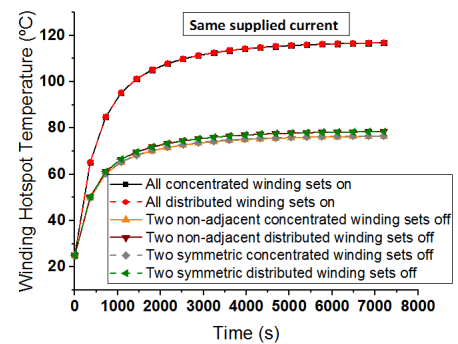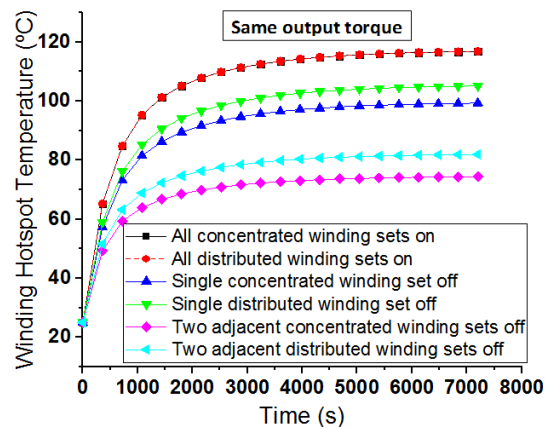
Similarly, Figure 10 presents the temperature distributions for the winding hotspots under normal and partial operating conditions (two non-adjacent and two symmetric three-phase winding sets off) for both winding topologies.

Meanwhile, the supplied currents to the three-phase winding sets without fault in the distributed modular three-phase winding topology must be increased to obtain the
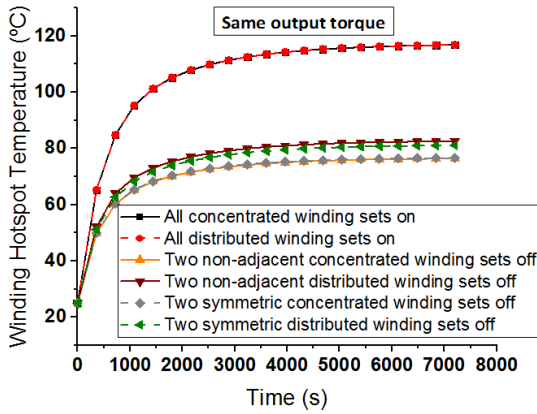
FIGURE 12. Windings hotspot temperature under same efficiency level for two non-adjacent and two symmetric three-phase winding sets partial operation.
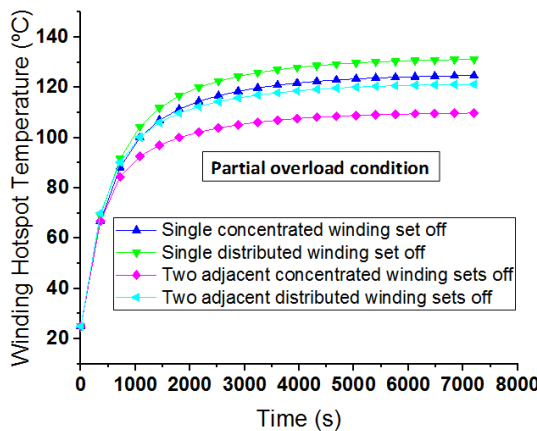

FIGURE 13. Windings hotspot temperature under partial overload condition (normal, single, and two adjacent three-phase winding sets off).

FIGURE 14. Windings hotspot temperature under partial overload condition (normal, single, and two adjacent three-phase winding sets off).

same efficiency level as the concentrated modular three-phase winding topology. Figures 11 and 12 present the temperature distributions for the winding hotspots when the supplied current to the distributed modular three-phase winding sets is increased to get the same torque level as the concentrated modular three-phase winding topology under the partial operation of the machine prototype. Moreover, the increased winding currents in the case of distributed modular three-phase winding topology result in comparatively higher winding hotspot temperature than the concentrated modular three-phase winding topology.

B. PARTIALLY OVERLOADED OPERATION AND MACHINE THERMAL BEHAVIOR UNDER MODULAR THREE-PHASE WINDING TOPOLOGIES

In order to make up for the lower efficiency under partial operation, this section investigates how the machine prototype performs under partially overloaded conditions by overloading the healthy three-phase winding sets. Figure 13 and Figure 14 illustrate the machine prototype thermal behavior under partially overloaded operation. It can
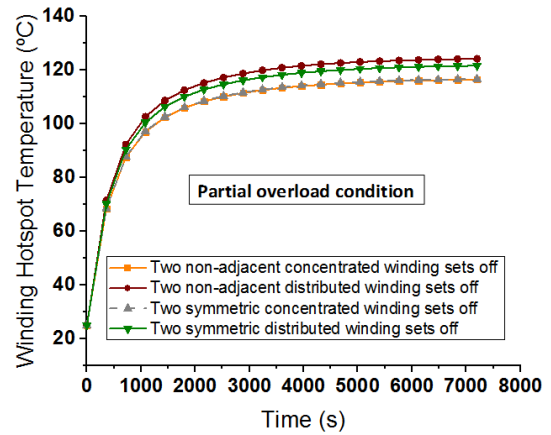
be observed that the temperature distribution in the active winding sets of the machine prototype has increased greatly for both the analyzed winding topologies under partially overloaded working conditions. This can eventually lead to the failure of the machine windings insulation or the PM's demagnetization. The next section presents the third type of modular three-phase winding topology and presents the comparative tabular data for the temperature distributions in different machine parts for all the analyzed modular three-phase winding topologies considering the machine's normal, partial and partially overloaded operation.

C. EFFICIENCY ANALYSIS AND THERMAL BEHAVIOR OF COMBINED CONCENTRATED AND DISTRIBUTED MODULAR THREE-PHASE WINDING TOPOLOGY

This section investigates the prototype machine's efficiency analysis and thermal behavior for the third type of winding topology using the coupled magnetic field and thermal analysis model. The third type of modular three-phase winding topology is shown in Figure 1(d), which combines the concentrated and distributed modular three-phase winding topologies. The machine model's normal healthy operation under the combined concentrated and distributed modular three-phase winding topology follows the same behavior as the individual concentrated and distributed modular three-phase winding topologies. However, there exist some differences in the partial working conditions for the combined concentrated and distributed modular winding topology compared to the other two analyzed winding topologies. Figure 15 presents the average torque waveform for the healthy operation and modular three-phase winding sets partial operation under the combined concentrated and distributed modular three-phase winding topology.

Moreover, Table 5 presents the average torque and torque ripples for the normal and partial operation of the combined concentrated and distributed modular three-phase winding topology. By comparing Table 5 and Table 2 from section 3, it can be observed that the average torque and torque

TABLE 5. Average torque and torque ripple under normal and partial operation for the combined concentrated and distributed modular three-phase winding topology.

| Machine operating conditions at rated current 77A (RMS)	Average Torque combined concentrated and distributed three-phase winding sets	% Torque Ripples
All three-phase winding sets working	93.1	0.107%
Single concentrated winding set off	77.7	0.097%
Single distributed winding set off	77.5	0.084%
Two non-adjacent concentrated winding sets off	62.2	0.094%
Two non-adjacent distributed winding sets off	61.8	0.107%
Two adjacent concentrated winding sets off	62.1	0.082%
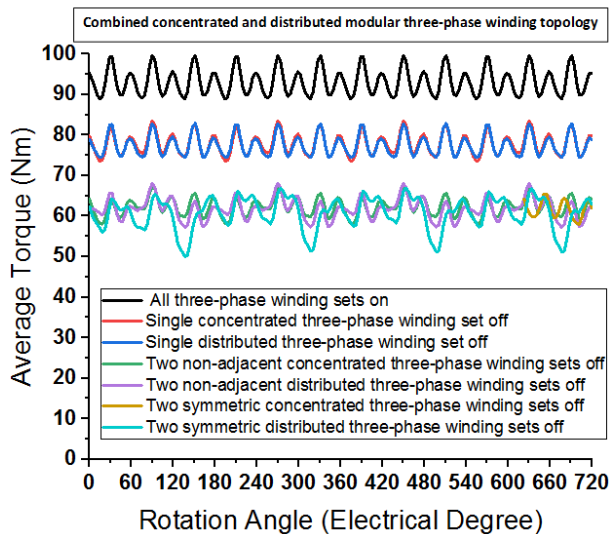
FIGURE 15. Average torque response for the combined concentrated and distributed modular three-phase winding topology.

FIGURE 16. Windings hotspot temperature under same efficiency level for the combined concentrated and distributed winding topology under normal, single, and two adjacent three-phase winding sets partial operation.

FIGURE 17. Windings hotspot temperature under same efficiency level for the combined concentrated and distributed winding topology under two non-adjacent and two symmetric three-phase winding sets partial operation.

ripples are almost the same for the concentrated modular three-phase winding topology and the combined concentrated and distributed modular three-phase winding topology when the same concentrated three-phase winding sets are turned off.

Figure 16 presents the windings hotspot temperature under the combined concentrated and distributed modular winding topology having the same efficiency level and applying the same technique as the previous two analyzed modular winding topologies under normal, single, and two adjacent three-phase winding sets partial operation. Similarly, the windings hotspot temperature under non-adjacent and symmetric two three-phase winding sets partial operation is presented in Figure 17 under the combined concentrated and distributed modular three-phase winding topology.

VI. COMPARATIVE THERMAL ANALYSIS OF MODULAR THREE-PHASE WINDING TOPOLOGIES

The comparative thermal behavior of the machine prototype with modular three-phase winding topologies is presented in this section for the windings hotspot temperature distribution using the coupled magnetic field and thermal model under normal and partial working conditions. Table 6 presents the
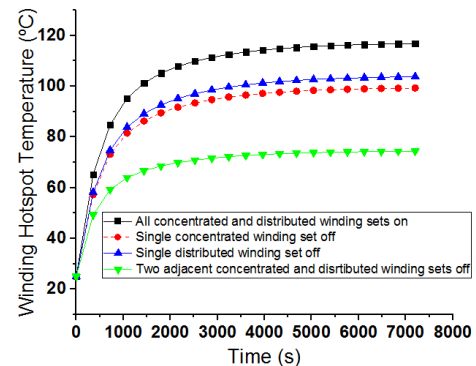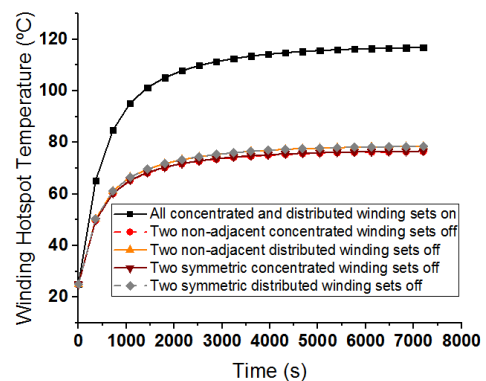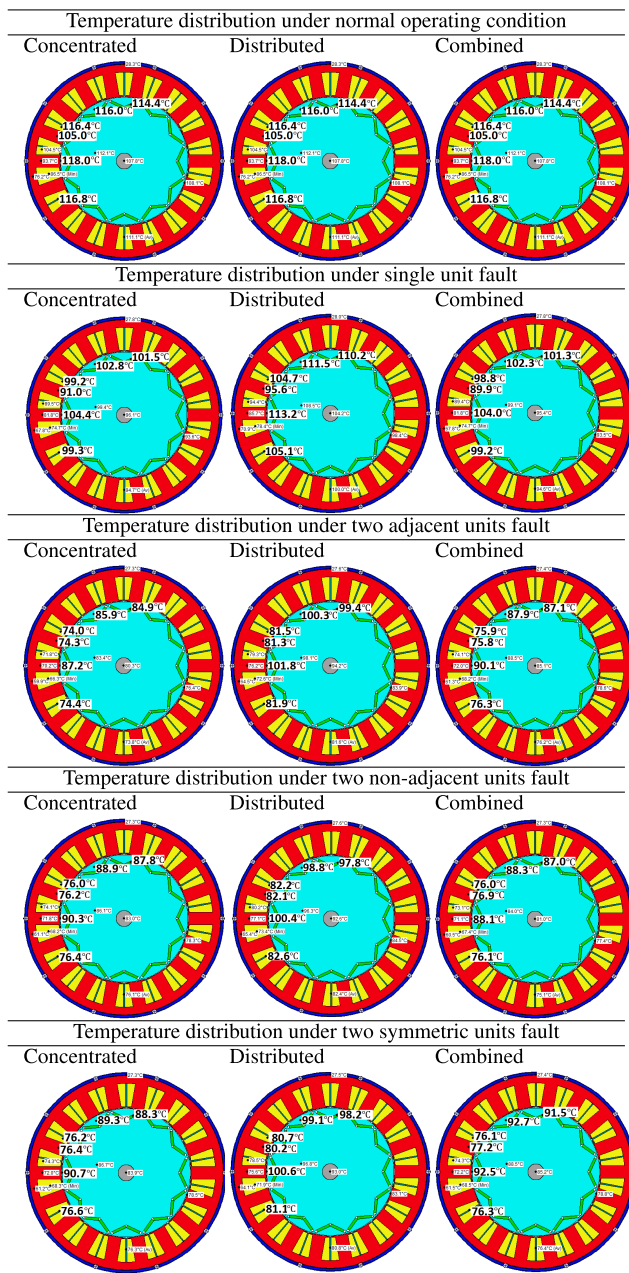
temperature distribution comparison data in the machine prototype various parts for the concentrated modular three-phase winding topology, distributed modular three-phase winding topology, and combined concentrated and distributed modular three-phase winding topology under normal and partial operation. The results obtained from these tables show that the temperature distribution under the normal working operation of the machine prototype with all the modular three-phase winding topologies is exactly the same; however, it is considerably different under the partial working operation.

TABLE 6. Modular three-phase winding topologies and machine temperature distribution under normal and partial working conditions.

TABLE 7. Modular three-phase winding topologies and machine temperature distribution under (partially overload) working conditions.

Similarly, Table 7 presents the temperature distribution data plots in various parts of the machine prototype under the partially overloaded working condition for the analyzed modular three-phase winding topologies. It has been shown that the winding hotspot temperature is considerably high under the partially overloaded working case for all the modular winding topologies, especially for the distributed modular three-phase winding topology. The high winding temperature distribution may result in winding insulation failure, resulting in safety issues and permanent damage to the machine. Henceforth, it is imperative to conduct a thermal

sensitivity analysis of the machine prototype, particularly under the partially overloaded situation for the analyzed winding topologies.

VII. MACHINE's PARTIALLY OVERLOADED OPERATION AND THERMAL SENSITIVITY ANALYSES UNDER THE MODULAR THREE-PHASE WINDING TOPOLOGIES

The thermal sensitivity analysis of the machine for the partially overloaded operation is conducted in this section focusing on a variety of thermal characteristics. Initially, the thermal parameters of the cooling system employed are examined to determine their impact on the machine thermal behavior under the analyzed winding topologies. Table 8 presents the optimal values for the thermal parameters. It also shows that the thermal parametric coefficients impact machine winding temperature to acquire appropriate values for thermal parameters. Similarly, the influence of the fluid volume flow rate, the height of the water, the water jacket width, spacing, and the lamination of the stator housing

S. H. Shah et al.: Coupled Magnetic Field and Thermal Analysis Model for IPMSM

IEEE Access

TABLE 8. Thermal parameters optimal values.

Parameters	Initial-value	Final value	Optimal value
Windings thermal conductivity ($W/m/°C$)	0.1	1.0	0.3
Housing surface natural convection heat coefficient ($W/m^2/°C$)	0.03	0.6	0.08
Heat transfer coefficient for air inside ($W/m^2/°C$)	1.5	1.8	1.3

TABLE 9. Thermal parametric sensitivity analysis and its effect on windings temperature under partial overload conditions.

Parameters	Initial-Final value	Optimal value	Initial Temp (°C)	Optimal Temp (°C)
Stator-Lam Housing (W/m/°C)	0.03-0.1	0.03	148.0	102.0
Water-jacket Channel-Lam (mm)	1-40	1	107.5	102.9
Water-jacket Channel-Height (mm)	1-40	3	110.6	101.7
Water-jacket Channel-Width (mm)	1-40	10	134.3	108.4
Water-jacket Channel-Spacing (mm)	1-40	10	114.2	109.5
Fluid volume flow rate (m^3/s)	$1.25e^{-5}$-$1.25e^{-2}$	$1.25e^{-2}$	130.4	87.9

are all examined for the used water-jacket cooling method. Table 9 presents the influence of the cooling method's thermal parameters on the machine thermal behavior under a single winding set open-circuit fault along with its optimized values.

Under the partially overloaded operation, the thermal sensitivity study results in selecting appropriate values for the thermal parameters, henceforth considerably decreasing the overheat difficulties of the machine prototype. Table 10 presents temperature distributions in various machine parts for the analyzed modular three-phase winding topologies under the partially overloaded operation and optimal thermal settings. It can still be observed that the distributed modular three-phase winding topology has the highest winding hotspot temperature distribution, while for the combined concentrated and distributed modular three-phase winding topology, the winding hotspot temperature distribution is considerably low by applying similar working conditions.

VIII. EXPERIMENTAL WORK
The machine's thermal behavior is validated through experimental work by comparing the optimized coupled magnetic field and thermal analysis results and the experimental test results of the machine prototype. Platinum (Pt) sensors are used for temperature measurement of the machine windings under different working conditions and modular

TABLE 10. Modular three-phase winding topologies and machine (thermal optimized) temperature distribution under partial overload working conditions.
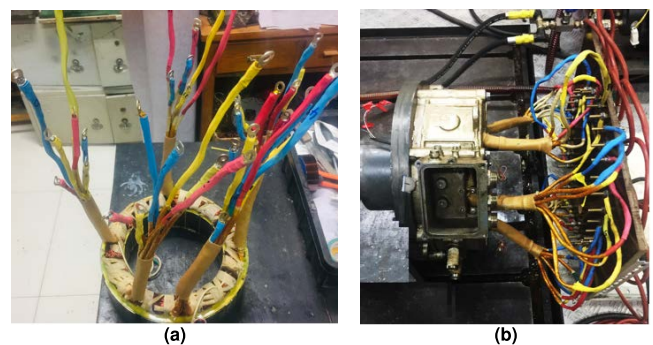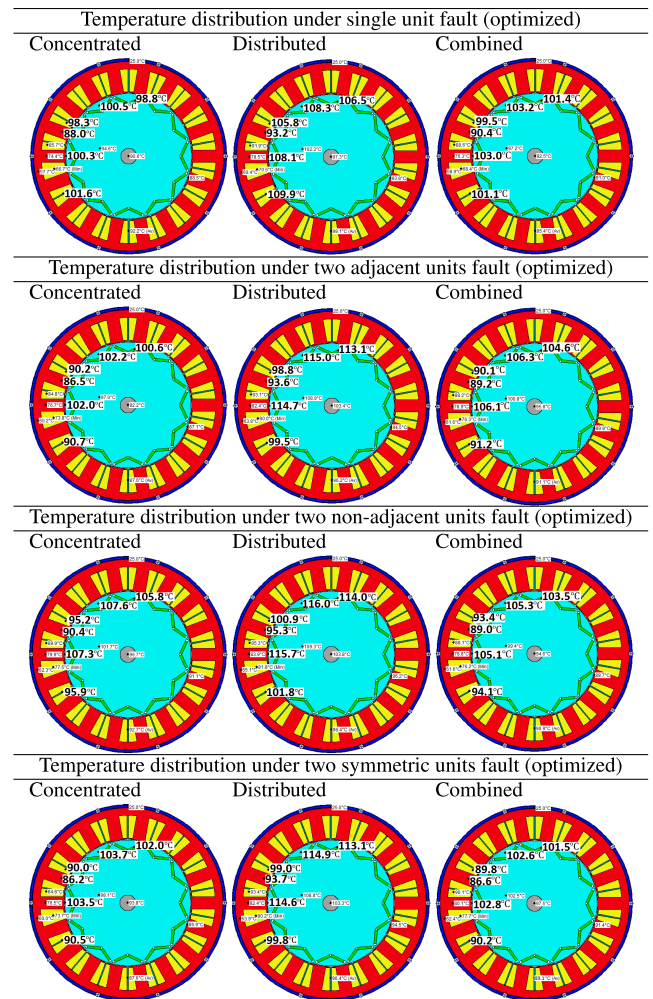

FIGURE 18. Machine model (a) winding process (b) Modular winding arrangement and experimental setup.

three-phase winding topologies. The manufacturing design of machine's modular three-phase winding and experimental platform are shown in Figures 18(a) and 18(b). Table 11 presents the windings hotspot temperature distribution data under different modular three-phase winding topologies for the machine's normal operation and partial operation.

VOLUME 10, 2022

30345

TABLE 11. Comparison of machine's steady-state thermal behavior under modular three-phase winding topologies.

Modular Concentrated Three-Phase Winding Sets	Parameters	All sets on	Partial operating conditions			
			Single set off	Two Adj set off	Two non-Adj set off	Two symmetric set off
	Rated Current (A)	77	77	77	77	77
	Joule losses (W)	1803	1533	1221	1271	1290
	Winding Max (T)°C	116.8[118.2]	99.3[101.4]	74.4[76.8]	76.4[78.3]	76.6[78.9]
Modular Distributed Three-Phase Winding Sets	Rated Current (A)	77	80	82	83	81
	Joule losses (W)	1803	1635	1407	1426	1389
	Winding Max (T)°C	116.8[118.6]	105.1[107.7]	81.9[83.2]	82.6[84.4]	81.1[83.9]
Combined concentrated and distributed Winding Sets (Concentrated sets off)	Rated Current (A)	77	77	77	77	77
	Joule losses (W)	1803	1517	1221	1271	1290
	Winding Max (T)°C	116.8[118.3]	99.2[101.8]	74.2[76.5]	75.4[77.9]	76.7[78.2]
Combined concentrated and distributed Winding Sets (Distributed sets off)	Rated Current (A)	77	77	77	77	77
	Joule losses (W)	1803	1533	1221	1271	1290
	Winding Max (T)°C	116.8[118.1]	103.8[104.2]	81.9[83.2]	82.6[84.2]	81.1[83.4]

TABLE 12. Comparison of machine's steady-state thermal behavior under modular three-phase winding topologies.

Modular Concentrated Three-Phase Winding Topology	Parameters	Partial overload working conditions (overload, optimized and experimental results)			
		Single set off	Two Adj set off	Two non-Adj set off	Two symmetric set off
	Rated Current (A)	95	128	128	128
	Joule losses (W)	1905	1955	2078	1967
	Winding Max (T)°C	125.7(101.6)[102.4]	109.7(90.7)[92.1]	116.4(95.9)[97.1]	116.7(90.5)[93.2]
Modular Distributed Three-Phase Winding Topology	Rated Current (A)	98	131	134	132
	Joule losses (W)	1989	2168	2226	2172
	Winding Max (T)°C	131.1(101.6)[102.4]	121.2(101.6)[102.4]	124.2(101.6)[102.4]	121.4(101.6)[102.4]
Combined concentrated and distributed Winding Sets (Concentrated sets off)	Rated Current (A)	95	128	128	128
	Joule losses (W)	1901	2012	2030	2081
	Winding Max (T)°C	125.1(101.6)[102.4]	118.8(101.6)[102.4]	116.0(101.6)[102.4]	116.3(101.6)[102.4]
Combined concentrated and distributed Winding Sets (Distributed sets off)	Rated Current (A)	95	128	128	128
	Joule losses (W)	2029	2037	2098	2019
	Winding Max (T)°C	125.1(101.1)[102.4]	111.8 (91.2)[93.1]	116.0(91.4)[93.4]	116.3(90.2)[92.5]

The normal working operation of the machine prototype with all the modular three-phase winding topologies is exactly the same. However, their partial working operation is considerably different. The values of winding hotspot temperature distribution given in square brackets in Table 11 are the experimental values for the machine prototype.

The obtained findings shows that the partial working operation of the distributed modular three-phase winding topology has the highest joule losses and winding hotspot temperature distribution to obtain the same efficiency level as the other two analyzed winding topologies under the same three-phase winding sets partial working conditions. Similarly, Table 12 presents comparison data for the windings hotspot temperature distribution under different modular three-phase winding topologies applying partially overloaded operation. The values of winding hotspot temperature distribution presented in small brackets in Table 12 are the optimized windings hotspot temperature values, while the values in square brackets are the experimental values for the winding hotspot temperature under optimized operating conditions of the machine prototype. The results presented in Table 12 shows that under the machine's partially overloaded operation, the distributed modular three-phase winding topology has the highest joule losses and winding hotspot temperature, while the combined concentrated and distributed modular three-phase winding topology has the lowest winding hotspot temperature and joule losses under the same working conditions

IX. CONCLUSION

This paper investigates the thermal behavior for multiple modular three-phase winding topologies of an IPMSM under healthy, partially working, and partially overloaded operations. The coupled electromagnetic FEA and thermal model approach has been used to investigate the machine prototype thermal behavior under different working cases and by applying multiple modular three-phase winding topologies. The calculated machine losses by applying electromagnetic FEA are coupled to the thermal (LPTN) model using the coupled electromagnetic FEA and thermal model approach to reliably estimate the temperature distribution in various components of a machine prototype, which are finally verified by experimental tests. The multiple research findings from this analysis are mentioned below

1) The thermal behavior of the machine prototype and the torque response under the healthy working conditions is the same for the concentrated modular three-phase, distributed modular three-phase, and combined concentrated and distributed modular three-phase winding topologies applying similar working conditions.

2) The thermal behavior and the torque response under the partial working conditions under multiple modular

three-phase winding topologies are different from each case under the same working conditions.

3) The temperature distribution in various machine parts, particularly winding hotspot temperature for the distributed modular three-phase winding topology under the partial working condition to obtain the same output torque, is considerably high, while for the combined concentrated and distributed modular three-phase winding topology is the lowest.

4) The thermal behavior of the machine prototype under the partially overloaded operation follows the same pattern with the highest winding temperature distribution for the distributed modular three-phase winding topology, while the lowest for the combined concentrated and distributed modular three-phase winding topology applying similar working conditions

5) Thermal parametric sensitivity analysis has been conducted for the machine's partially overloaded operation for all the analyzed modular three-phase windings topologies to optimize the temperature distribution in various machine's parts, particularly the winding hotspot temperature under partial overloaded conditions. Experimental tests verify the optimized values for the windings hotspot temperature for all modular three-phase winding topologies.

It can be concluded that the coupled magnetic field and thermal analysis approach can be used effectively to investigate the thermal behavior of the modular designed IPMSM. similarly from the findings mentioned above it can be seen that under the machine's partial and partially overloaded operation, the machine's thermal behavior and efficiency performance are comparatively better for the concentrated modular three-phase winding topology than the distributed modular three-phase winding topology. Moreover, the advantages of the concentrated modular three-phase and distributed modular three-phase winding topology can be used together to form the combined concentrated and distributed modular three-phase winding topology, which can be considered as an alternative choice with better thermal behavior and efficiency performance compared to the individual concentrated modular and distributed modular three-phase winding topology under partial and partially overloaded operations for applications requiring fault-tolerance.

REFERENCES

[1] M. J. Duran and F. Barrero, "Recent advances in the design, modeling, and control of multiphase machines—Part II," *IEEE Trans. Ind. Electron.*, vol. 63, no. 1, pp. 459–468, Jan. 2016.

[2] E. Levi, "Multiphase electric machines for variable-speed applications," *IEEE Trans. Ind. Electron.*, vol. 55, no. 5, pp. 1893–1909, May 2008.

[3] P. Taras, G.-J. Li, Z.-Q. Zhu, M. P. Foster, and D. A. Stone, "Combined multiphysics model of switched flux PM machines under fault operations," *IEEE Trans. Ind. Electron.*, vol. 66, no. 9, pp. 6737–6745, Sep. 2019.

[4] I. Zoric, M. Jones, and E. Levi, "Arbitrary power sharing among three-phase winding sets of multiphase machines," *IEEE Trans. Ind. Electron.*, vol. 65, no. 2, pp. 1128–1139, Feb. 2018.

[5] L. Alberti and N. Bianchi, "Impact of winding arrangement in dual 3-phase induction motor for fault tolerant applications," in *Proc. 21th Int. Conf. Electr. Mach. (ICEM)*, Sep. 2010, pp. 1–6.

[6] E. Levi, F. Barrero, and M. J. Duran, "Multiphase machines and drives—Revisited," *IEEE Trans. Ind. Electron.*, vol. 63, no. 1, pp. 429–432, Jan. 2016.

[7] P. Zhou, D. Lin, Y. Xiao, N. Lambert, and M. A. Rahman, "Temperature-dependent demagnetization model of permanent magnets for finite element analysis," *IEEE Trans. Magn.*, vol. 48, no. 2, pp. 1031–1034, Feb. 2012.

[8] G. J. Li, J. Ojeda, E. Hoang, and M. Gabsi, "Thermal-electromagnetic analysis of a fault-tolerant dual-star flux-switching permanent magnet motor for critical applications," *IET Electr. Power Appl.* vol. 5, no. 6, pp. 503–513, 2011.

[9] P. H. Mellor, D. Roberts, and D. R. Turner, "Lumped parameter thermal model for electrical machines of TEFC design," *IEE Proc. B Electr. Power Appl.*, vol. 138, no. 5, p. 205, 1991.

[10] M. Popescu, D. G. Dorrell, L. Alberti, N. Bianchi, D. A. Staton, and D. Hawkins, "Thermal analysis of duplex three-phase induction motor under fault operating conditions," *IEEE Trans. Ind. Appl.*, vol. 49, no. 4, pp. 1523–1530, Jul. 2013.

[11] M. Cheng, J. Wang, S. Zhu, and W. Wang, "Loss calculation and thermal analysis for nine-phase flux switching permanent magnet machine," *IEEE Trans. Energy Convers.*, vol. 33, no. 4, pp. 2133–2142, Dec. 2018.

[12] H. Zhang, P. Giangrande, G. Sala, Z. Xu, W. Hua, V. Madonna, D. Gerada, and C. Gerada, "Thermal model approach to multisector three-phase electrical machines," *IEEE Trans. Ind. Electron.*, vol. 68, no. 4, pp. 2919–2930, Apr. 2021.

[13] G. J. Li, J. Ojeda, E. Hoang, and M. Gabsi, "Thermal-electromagnetic analysis of a fault-tolerant dual-star flux-switching permanent magnet motor for critical applications," *IET Electr. Power Appl.* vol. 5, no. 6, pp. 503–513, no. 2011.

[14] W. Yu, W. Hua, J. Qi, H. Zhang, G. Zhang, H. Xiao, S. Xu, and G. Ma, "Coupled magnetic field-thermal network analysis of modular-spoke-type permanent-magnet machine for electric motorcycle," *IEEE Trans. Energy Convers.*, vol. 36, no. 1, pp. 120–130, Mar. 2021.

[15] S. H. Shah, X. Wang, U. Abubakar, L. Wang, and P. Gao, "Investigation of noise and vibration characteristics of an IPMSM with modular-type winding arrangements having three-phase sub-modules for fault-tolerant applications," *IET Electr. Power Appl.*, vol. 16, no. 2, pp. 248–266, Feb. 2022, doi: 10.1049/elp2.12150.

[16] S. H. Shah, X. Wang, M. Azeem, and U. Abubakar, "Evaluation of magnetomotive force and torque ripples in modular type IPMSM with multi three-phase winding configurations," *IEEE Access*, vol. 10, pp. 1577–1590, 2022, doi: 10.1109/ACCESS.2021.3138727.

[17] Y. Sui, P. Zheng, F. Wu, P. Wang, L. Cheng, and J. Zhu, "A novel five-phase fault-tolerant modular in-wheel permanent-magnet synchronous machine for electric vehicles," *J. Appl. Phys.*, vol. 117, no. 17, May 2015, Art. no. 17B521.

[18] P. Giangrande, V. Madonna, S. Nuzzo, C. Spagnolo, C. Gerada, and M. Galea, "Reduced order lumped parameter thermal network for dual three-phase permanent magnet machines," in *Proc. IEEE Workshop Electr. Mach. Design, Control Diagnosis (WEMDCD)*, Apr. 2019, pp. 71–76.

[19] P. Pescetto, S. Ferrari, G. Pellegrino, E. Carpaneto, and A. Boglietti, "Winding thermal modeling and parameters identification for multitthree phase machines based on short-time transient tests," *IEEE Trans. Ind. Appl.*, vol. 56, no. 3, pp. 2472–2480, May 2020.

[20] A. Boglietti, M. Cossale, M. Popescu, and D. A. Staton, "Electrical machines thermal model: Advanced calibration techniques," *IEEE Trans. Ind. Appl.*, vol. 55, no. 3, pp. 2620–2628, May 2019, doi: 10.1109/TIA.2019.2897264.

[21] S. H. Shah, X. Wang, U. Abubakar, and S. ur Rehman, "Thermal parametric sensitivity analysis of an IPMSM with multi three-phase sector windings topology under normal, partial and partial overload operating conditions," in *Proc. IEEE Ind. Electron. Appl. Conf. (IEACon)*, Nov. 2021, pp. 85–90, doi: 10.1109/IEACon51066.2021.9654695.

[22] U. Abubakar, X. Wang, S. H. Shah, and S. Ur Rahman, "Parametric thermal sensitivity analysis of 225kW high speed PMSM for blower application," in *Proc. IEEE Ind. Electron. Appl. Conf. (IEACon)*, Nov. 2021, pp. 97–102, doi: 10.1109/IEACon51066.2021.9654499.

[23] S. H. Shah, X. Wang, U. Abubakar, and P. Gao, "Analysis of the radial component of electromagnetic force density and vibration behavior of an IPMSM with multiple three-phase winding units," in *Proc. IEEE Ind. Electron. Appl. Conf. (IEACon)*, Nov. 2021, pp. 246–251, doi: 10.1109/IEACon51066.2021.9654698.

SAYYED HALEEM SHAH was born in Islamabad, Pakistan. He received the B.Sc. degree in electrical engineering from the University of Engineering and Technology, Peshawar, Pakistan, in 2011, and the M.S. degree in electrical engineering from Air University, Islamabad, Pakistan, in 2014. He is currently pursuing the Ph.D. degree in electrical engineering with the School of Electrical and Information Engineering, Tianjin University, China. His research interests include electrical machine design, modular type machines, and noise and vibration in modular type machines.

MUHAMMAD AZEEM was born in Pakistan. He received the B.Sc. degree in electrical engineering from the Federal Urdu University of Arts, Science and Technology, Islamabad, Pakistan, in 2015, and the M.S. and Ph.D. degrees in electrical engineering from Kunsan National University, Gunsan, South Korea, in 2018 and 2021, respectively. His research interests include electrical machine design, permanent magnet machines, and flux modulation machines.

XIAOYUAN WANG was born in Hebei, China, in 1962. He received the B.S. and M.S. degrees in electrical engineering from Tianjin University, Tianjin, China, in 1982 and 1985, respectively, and the Ph.D. degree in electrical engineering from the Shenyang University of Technology, Shenyang, China, in 2006. He has been working as a Professor at the School of Electrical and Information Engineering, Tianjin University, since 2007. His current research interests include electrical machine design, and motor drives system for high speed applications.

USMAN ABUBAKAR was born in Kano, Nigeria. He received the B.Eng. degree in electrical engineering from the Kano University of Science and Technology, Wudil, Nigeria, in 2011, and the M.Eng. degree in electrical engineering from the Liaoning University of Technology, Jinzhou, China, in 2014. He is currently pursuing the Ph.D. degree in electrical engineering with Tianjin University. His research interests include the design of a cooling system and thermal analysis of high-speed PMSM.

• • •